

Physics-Informed LSTM Networks for High-Accuracy Transient Prediction of Marine IRGT/SOFC Under Sudden Load Decreasing[#]

Jiale Wen¹, Shengying Xiao¹, Yubo Yao¹, Xicong Mi¹, Catalina Spataru², Yiwu Weng³, Xiaojing Lv^{1*}

1 China-UK Low Carbon College, Shanghai Jiao Tong University, Shanghai, 201306, China

2 Energy Institute, University College London, London, WC1H0NN, United Kingdom

3 School of Mechanical Engineering, Shanghai Jiao Tong University, Shanghai, 200240, China

*(Corresponding Author: lvxiaojing@sjtu.edu.cn)

ABSTRACT

To address the challenge of rotor speed drift, large overshoot, and even DC microgrid instability caused by constant generator rotor speed inaccurate prediction in marine IRGT/SOFC all-electric propulsion systems, this study proposes a physics-informed Long Short-Term Memory framework to enhance transient prediction accuracy and robustness. This method integrates rotor nonlinear differential equations into the loss function, enforcing physical characteristic consistency while leveraging the LSTM memory capability to capture long-term nonlinear dependencies. The dataset from the mechanism and data-driven hybrid model which is validated in 2.5% error by experiment is used for training.

Results demonstrate that it reduces 55% Root Mean Square Error for key power parameters of system output power, with RMSE dropping from 107 to 52 and 183 to 83, respectively. For generator rotor speed, the RMSE improved by 50%, from 2.08 to 1.05, with an R^2 increase from 0.926 to 0.998, which mitigate rotor speed drift and overshoot, ensuring accurate and reliable predictions. Under dynamic conditions such as sudden load decreases, the PI-LSTM framework maintains stability and limits the prediction error for generator rotor speed to a maximum of 5 rpm, while the traditional LSTM suffers deviations as large as 30 rpm (1%). This work introduces a novel technical approach for next-generation marine hybrid propulsion systems, enabling highly accurate dynamic predictions and enhancing the reliability of marine microgrid operations.

Keywords: Dynamic prediction, Physics-Informed LSTM, IRGT/SOFC hybrid system, all-electric propulsion, constant-speed generation

NONMENCLATURE

Abbreviations

IRGT	Intercooled reheat gas turbine
SOFC	Solid oxide fuel cell

PI-LSTM	Physics-Informed Long Short-Term Memory
IMO	International Maritime Organization
IPS	Integrated power system
LPC	Low-pressure compressor
HPC	High-pressure compressor
CC	Combustion chamber
HPT	High-pressure turbine
LPT	Low-pressure turbine
PT	Power turbine
HE	Heat exchanger
CCC	Catalytic combustion chamber
P-R	Pre-reformer
CR	Cracker
G	Generator
TIT	Turbine inlet temperature(K)
PTOT	Power turbine outlet temperature(K)
S/C	Steam carbon ratio
C	Carbon decomposition rate
ADAM	Adaptive Moment Estimation
RMSE	Root Mean Squared Error
MAE	Mean Absolute Error
R^2	Multiple determination coefficient

1. INTRODUCTION

With the rapid development of the global maritime transportation and the increasingly rigorous IMO regulations^[1], large ocean-going ships electrification has gained unprecedented momentum^[2]. The all-electric propulsion system with a DC distribution has gradually emerged as a transformative solution for ocean-going vessels due to its advantages such as energy diversity, high space utilization, and flexible layout^[3, 4]. Its primary power sources include gas turbines^[5], diesel engines^[6], and batteries^[7]. However, diesel engines and gas turbines have low efficiency and high emissions, while the endurance of batteries is limited, all of which fail to

meet the future demand for all-electric and low-carbon development in maritime applications.

The SOFC/GT hybrid system has gained widespread attention due to its characteristics such as high efficiency above 60%^[8], low noise^[9], and strong fuel adaptability^[10, 11]. Combining the high efficiency and low emissions of SOFC with the rapid power response and high-power density of gas turbines, this system significantly improves vessel range while enabling fast mode switching during navigation, making it a promising solution for next-generation all-electric propulsion systems for ships^[12, 13]. Although many researchers have conducted studies on

methods by training on large datasets, improving speed prediction accuracy. It is evident that, whether through mechanistic modeling or data-driven approaches, there is still a gap in the precise prediction of the generator rotor in all-electric ship SOFC/GT power generation systems. It leads to generator rotor speed drift, large overshoot, degraded control performance, and even risks of DC bus voltage collapse during load transients.

Nevertheless, existing studies focus on either simple rotor models or purely transient dynamics of SOFC or GT prediction, ignoring their coupled characteristic to DC marine microgrid under constant-speed generation

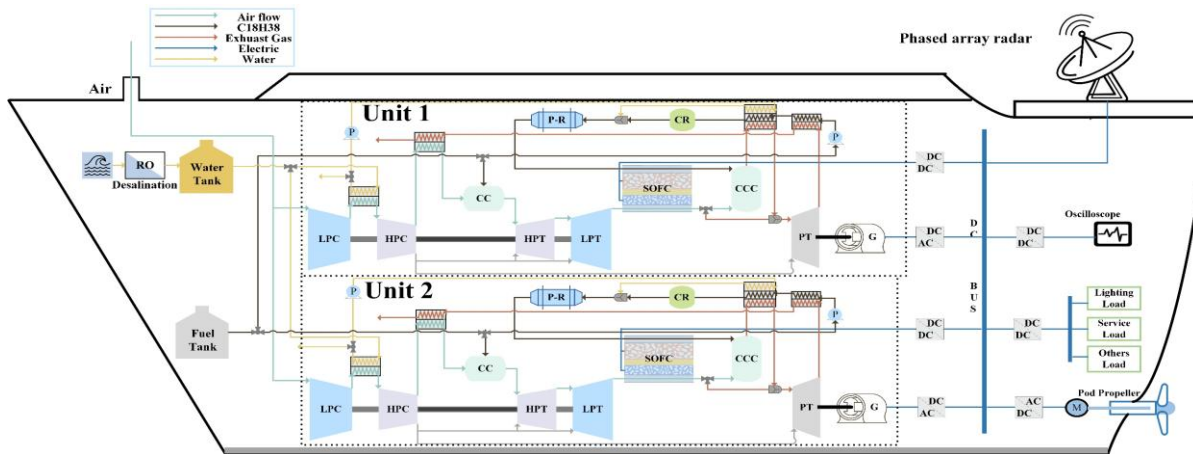


Fig. 1 Structural diagram of all-electric IRGT/SOFC hybrid system on ship

system mechanisms, data predictions^[14], and predictive control^[15-17] with favorable results, key issues in all-electric ship propulsion systems have been overlooked, particularly the study of turbine-generator constant generation speed operation characteristics. Panday et al.^[18] analyzed the constant-speed operational performance of the gas turbine generator in an SOFC/GT hybrid system through thermodynamic modeling, showing that variations in speed can significantly affect the system's performance and the stability of the microgrid. Therefore, to achieve accurate dynamic predictions of hybrid power systems under all-electric propulsion, it is crucial to accurately characterize the transient dynamic behavior of the constant-speed rotor connecting the generator and gas turbine.

To address this issue, some researchers have focused on predicting gas turbine power generation performance under all-electric conditions. Haji et al.^[19] proposed an adaptive model predictive control method for the V94.2 gas turbine power generation system, effectively improving system control precision and stability. Fadja et al.^[20] proposed a machine learning-based method for predicting constant-speed variations of gas turbines, which avoids the complexity of traditional modeling

constraints. Moreover, PINN lack the ability to capture long-term transient characteristic, which is essential for hybrid systems with multi-timescale dynamics.

This study employs the PI-LSTM method for the marine IRGT/SOFC all electric propulsion system, incorporating the rotor physical constraints into the data modeling process. A data-mechanism hybrid driven model is developed to produce the training data and predict the dynamic response of the system. The accuracy and robustness of the PI-LSTM based hybrid system model is analyzed comparing with the typical LSTM and BP predict model.

2. MODELING METHODOLOGY

2.1 Data-mechanism hybrid driven model

A representative 68 MW all-electric ocean-going vessel^[21] is selected for modeling and simulation, designed to support a propulsion load of 56 MW and auxiliary high-power electrical loads of 12 MW. As illustrated in Fig. 1, the propulsion system comprises two identical 34 MW hybrid units, each integrating a 24 MW IRGT and a 10 MW SOFC stack. Additional subsystems include a pre-reformer, cracker, catalytic combustion chamber, heat exchanger, and generator. AC outputs from the IRGT are rectified through AC/DC inverters and

distributed via a 4 kV DC bus. The above mechanism and data-driven hybrid static model work have been described in detail in previous studies^[22], and this paper will presents the dynamic models of key components.

2.2 Dynamic modeling

2.1.1 GT dynamic modeling

The transient model of gas turbine part has been completed in the previous research^[23], mainly including three shaft power balance, energy balance, mass balance, and volume dynamic model. When the load continuously decreases by 20% to 20% rated load condition, the maximum error of power rotor overshoot between the

established gas turbine dynamic model and the experimental data does not exceed 0.12%.

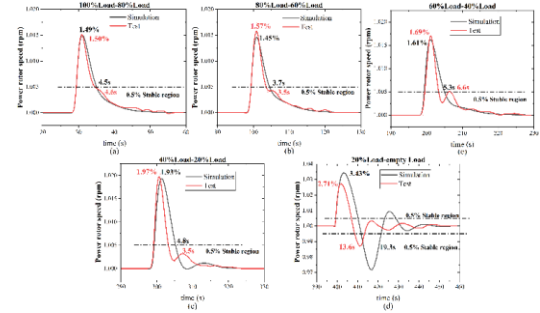


Fig. 2 Simulation and test comparison for PT rotor speed of the gas turbine under load step

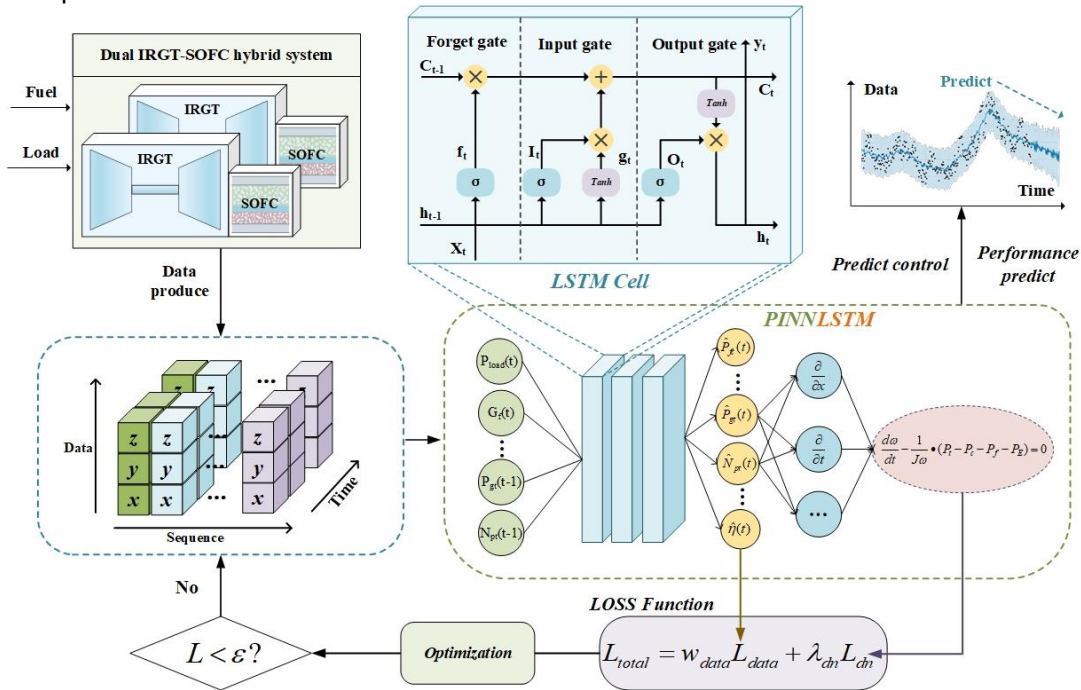


Fig. 3 IRGT/SOFC with generation rotor PI-LSTM prediction model structure

2.1.2 SOFC dynamic modeling

The model adopts an anode-supported, direct internal reforming SOFC stack design, referencing commercial designs from Bloom Energy^[24]. Each stack comprises 450 single cells. The model includes: a thermodynamic sub-model to simulate temperature, heat and mass transfer. an electrochemical sub-model incorporating polarization, ohmic, and concentration losses. Previous studies from our group provide the basis dynamic modeling work and validation^[25]. As shown in , the SOFC model is benchmarked using step-change response tests, with transient error within 0.8% as shown in Fig.3^[26], confirming its accuracy.

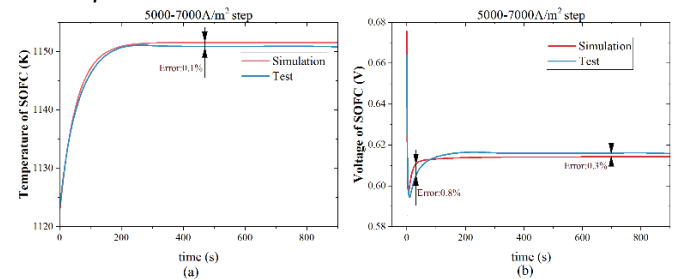


Fig. 4 Transient response of SOFC voltage(a) and temperature output (b) for 5000A/m² to 7000A/m²^[26]

2.1.3 Diesel cracking and reforming model

Liquid diesel is selected as the fuel for compatibility with existing marine infrastructure. It is reformed into hydrogen-rich gas using cracking techniques. The complex diesel composition is simplified to C₁₈H₃₈ for modeling. This dynamic model builds on previous research conducted by our team^[25].

2.1.4 Constraint and Design Parameters

The following key constraint conditions need to be considered. The boundary conditions for the model are shown in Table 1^[26]. According to selected type ship and above mathematic modeling approach, the main modeling parameters employed in the hybrid system are shown in Table 2.

Table 1 Safety constrains for key components

Parameter	Constraint
Power Turbine Temp. T_{exGT}	<1073K
LPC Surge Margin SM_{LPC}	>10%
SOFC Temp. T_{FC}	<1273
CCC Temp. T_{CCC}	<1473K
SOFC Temp. Gradient T_{FCavg}	<10K/cm
Carbon Deposition Rate C	<5mol/s

Table 2 IRGT/SOFC hybrid system design parameters

Parameters	Value	Parameters	Value
LPC pressure ratio	4.4	Slices/stack	450
HPC pressure ratio	4.55	Stack number	288
Rotor efficiency	99%	S/C	1.54
Inlet air flow rate	104.6kg/s	Current density	5500A/m ²
TIT	1550K	SOFC pressure	560kPa
C ₁₈ H ₃₈ LHV	47270kJ/kg	Fuel utilization	75%
Anode thickness	0.5mm	Cathode thickness	0.05mm
LPC efficiency	85%	Electrolyte thickness	0.02mm
HPC efficiency	85.8%	Length	0.4m
Volume loss	1-2%	Width	0.1m
HE pressure loss	1-3%	SOFC pressure loss	1-3%
CC, CCC loss	1-5%	Pre-reformer loss	1-5%
Generator efficiency	99%	AC/DC efficiency	99%
Volume	10m ³	Rotor inertia (HP, LP)	200kg/m ²

3. PI-LSTM IDENTIFICATION MODELING

3.1 Data source preparation

Based on the established model, a large amount of transient simulation data is generated by adjusting the fuel flow input to simulate different load disturbance processes. Fuel flow disturbances with different amplitudes and rates are injected to ensure that the dataset not only covers steady-state points but also includes dynamic processes under acceleration, deceleration, and disturbances. To avoid safety issues caused by excessively fuel mutation, this paper designs a piecewise linear constrained signal generator, which takes values within a preset minimum/maximum range based on the current fuel value to restrict fuel flow.

Table 3 Data generation setting work

Item	Variables	Range or setting
Input	Range of fuel flow	0.14 – 1.57 kg/s
	Random interval time	100 – 500 s
	Fuel limit threshold	[0.2, 0.25, 0.35, 0.5, 1.43, 1.57]
	Fuel limit	[0.2, 0.3, 0.4, 0.5, 0.8, 0.8]
Setting	Sampling time	0.01 s
	Duration	≥ 10000 s
	Data scale	~10 ⁶

3.2 Data processing methods

All input and output variables are normalized to the range [-1, 1] using global Min-Max scaling to reduce unit inconsistency and enhance convergence. The dataset is randomly split into training (80%), validation (10%), and test (10%) sets. To improve training efficiency and memory utilization, long time series are divided into fixed-length subsequences, forming training samples.

$$x_{norm} = \frac{2(x - x_{min})}{x_{max} - x_{min}} - 1 \quad (1)$$

$$XTrain_i = \{u_{(i-1)L+1}, u_{(i-1)L+2} \dots u_{iL}\} \quad (2)$$

3.3 PI-LSTM Model description

The dynamic response is often represented as a trend-type time series. LSTM is an enhanced Recurrent Neural Network that focuses on capturing the long-term and short-term dependencies of time-series data. It is distinguished by the integration of three gating mechanisms and a memory cell. The main calculation process of LSTM is about forget gate, input gate and output gate computation process, which are shown as below equations from (4) to (9). Among them, σ is the sigmoid activation function. LSTM can effectively handle the temporal dependencies of the system by dynamically updating the cell state c_t and the hidden state h_t through the gating mechanism.

$$i_t = \sigma(W_{ii}x_t + b_{ii} + W_{hi}h_i + b_{hi}) \quad (3)$$

$$f_t = \sigma(W_{if}x_t + b_{if} + W_{hf}h_{i-1} + b_{hf}) \quad (4)$$

$$g_t = \tanh(W_{ig}x_t + b_{ig} + W_{hg}h_{i-1} + b_{hg}) \quad (5)$$

$$o_t = \sigma(W_{io}x_t + b_{io} + W_{ho}h_{i-1} + b_{ho}) \quad (6)$$

$$c_t = f_t \odot c_{t-1} + i_t \odot g_t \quad (7)$$

$$h_t = o_t \odot \tanh(c_t) \quad (8)$$

LSTM is effective at handling time series data, but it is highly data dependent. When data is limited, it often leads to a lack of generalization and the risk of ignoring physical laws. To address this limitation, PI-LSTM, a method combining LSTM with PINN is proposed. This methodology incorporates the fundamental principles of physics into the training process, enabling the model to adhere to constraints such as energy conservation in a data-driven manner. Specifically, PINN is a neural network model that integrates data-driven techniques with the physical laws. This integration is achieved by incorporating both the physical residual terms and data-driven terms into the loss function, thereby facilitating the fusion of data and physical information.

3.4 Loss function design

As shown in equation 9, the loss function is constructed as a weighted sum of data error and a physics-informed residual term. The data loss L_{data} is defined as the mean squared error (MSE) between the predicted outputs and measured ground truth in the normalized space in equation 10. The physics residual loss L_{dn} incorporates the governing equation of rotor dynamics under constant-speed generation in equation 11. w_{data} and λ_{dn} represent the weights of data errors and physical errors. y_i , \hat{y}_i , and n represent real value, predict value and sample size. where n is the rotor speed, J is the inertia, P_{gt} is the turbine output power of gas turbine, and P_{load} is the marine microgrid load.

$$L_{total} = w_{data}L_{data} + \lambda_{dn}L_{dn} \quad (9)$$

$$L_{data} = \frac{1}{N} \sum_{i=1}^N |y_i - \hat{y}_i| \quad (10)$$

$$L_{dn} = \frac{1}{N-1} \sum_{t=2}^N \left(\frac{n(t) - n(t-1)}{dt} - \frac{900}{J\pi^2 n(t)} (P_{gt}(t) - P_{load}(t)) \right)^2 \quad (11)$$

3.5 Hyperparameter Selection

In training PI-LSTM networks, hyperparameter optimization is crucial for deep learning, which directly affects the convergence speed and final performance of the model. Hyperparameter optimization algorithms can be broadly classified into three main categories: grid search, random search, and Bayesian optimization. Through random search method, this paper mainly

optimizes and decide the following hyperparameters: sampling time, number of LSTM layers, number of neurons, and learning rate. Table 4 summarizes the key network settings.

Table 4 PI-LSTM Hyperparameter Settings

Category	Name	Value
Structure	Input layer neurons number	12
	Output layer neurons number	10
	Hidden layer number	3
	Hidden layer neurons number	50, 50, 50
	Length of sequence	2000
	Maximum training epochs	2000
Training	Optimizer	ADAM
	Cost function	L_{total}
	w_{data}, λ_{dn}	1, 0.5

4. RESULTS AND ANALYZE Validation and comparison of the PI-LSTM model

We selected sixteen groups of high-quality step fuel dynamic data from the dataset, which consisted of approximately 800,000 time-series data points. After preprocessing and standardization, 12 groups were used for training, 2 for testing, and 2 for validation. Table 5 compares the training time, prediction time, and memory costs of both the PI-LSTM and LSTM models under the same hyperparameter settings.

As shown in Table 5, while the PI-LSTM requires significantly more training time and slightly higher memory costs than the LSTM, these differences are attributable to the inclusion of physical constraints in the PI-LSTM model, which necessitates additional computational resources. Despite this, the prediction times for both models are nearly identical, indicating that the inclusion of physical laws does not introduce substantial delays in the inference phase.

Table 5 The training, prediction time and memory cost

Model	PI-LSTM	LSTM	PI-LSTM	LSTM
	Training	Training	Prediction	Prediction
Time	434min	126min	2.69s	2.81s
Memory	11GbGPU	9GbGPU	/	/

The introduction of physics-informed constraints in the PI-LSTM model significantly reduces the prediction errors across nearly all observed parameters. Table 6 and Figure 5 highlight these improvements:

The Root Mean Square Error (RMSE) for power parameters, such as P_{fcout} and P_{gtout} , decreased by 55%, from 107 to 52 and from 183 to 83, respectively. The RMSE for T_{extg} , T_{fc} , and T_{ccc} decreased by up to 62%, dropping from 2.53, 1.53, and 2.21 to 1.31, 0.68,

and 0.83, respectively. The RMSE for C dropped by 50%, from approximately 0.04 to 0.02. Despite already low error values, PI-LSTM further reduced the RMSE of Eff from 0.04 to 0.03. The RMSE for Rotor decreased by around 50%, from 2.08 to 1.05, with an R^2 increase from 0.926 to 0.998—7.7% improvement. These results confirm that the PI-LSTM's incorporation of physical constraints effectively mitigates the drift and overshoot associated with inertia, leading to higher accuracy in the prediction of system performance.

Table 6 Comparison of Training Metrics

Variable	MSE		RMSE		R^2	
	0.5	0	0.5	0	0.5	0
λ_{dn}						
Pfcout	2683	11656	51.8	107	0.999	0.995
Pgtout	6865	33493	82.8	183	0.999	0.999
Eff	1e-5	1e-4	0.03	0.04	0.998	0.988
Texgt	1.72	6.26	1.31	2.5	0.999	0.997
Tfc	0.47	2.34	0.68	1.53	0.999	0.994
SurgeLC	1e-5	1e-6	0.01	0.01	0.999	0.984
C	0.0003	0.001	0.02	0.04	0.999	0.992
Tfcavg	0.002	0.01	0.04	0.11	0.998	0.972
Tccc	0.69	4.89	0.83	2.21	0.999	0.988
Rotor	1.1	4.36	1.05	2.08	0.998	0.926

Figure 6 presents scatter plots comparing the predicted versus real values for key system variables: output power and rotor speed. PI-LSTM exhibits superior predictive accuracy, with data points clustered closer to the diagonal, indicating that its predictions are more consistent with real-world measurements. In contrast, LSTM demonstrates a greater spread, especially in low-power regions, reflecting its weaker ability to model power dynamics under variable conditions.

Moreover, the rotor speed fluctuations are better captured by PI-LSTM, with less deviation from the actual values, suggesting that it offers improved stability and response under dynamic conditions.

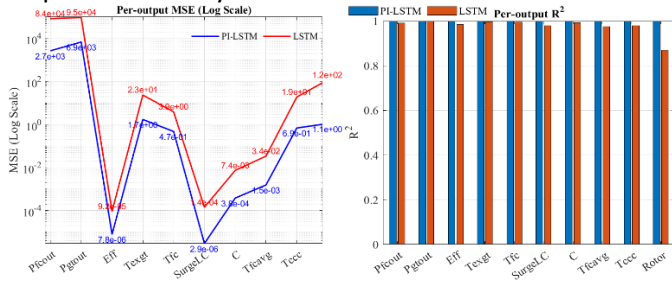


Fig. 5 Comparison of MS, R2 under Multi-parameter

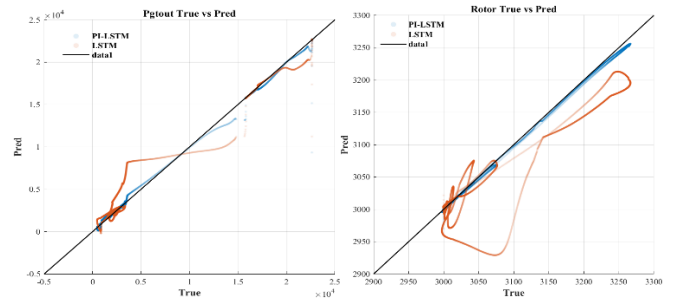


Fig. 6 Scatter plot of power and rotor speed prediction

4.2 Scenario of continuously sudden load decrease

During ship navigation, a sudden reduction in the propulsion system's load, system disconnection can trigger an abrupt decrease in the power grid load of the power system. In order to simulate the predictive behavior and generalization of the system in the case of continually sudden load drop, the hybrid system is operated at 68 MW in the initial state, while the demand load of the grid drops sharply to 54.4 MW, 40.8MW and 27.2MW. The power distribution strategy between SOFC and GT follows the previous work of the research group[22].

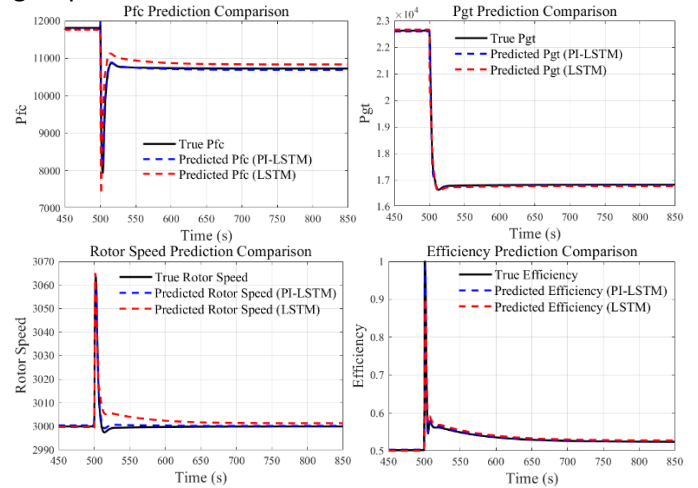


Fig. 7 Prediction Characteristics of SOFC, GT Power, Generation rotor speed, and efficiency based on PI-LSTM and LSTM under 100%-80% load variation

It can be seen from Figure 7 that under sudden load change, the SOFC power decreases rapidly and then rises back to 10.8MW, the gas turbine power drops rapidly to 16.6MW, and the maximum speed overshoot is 65rpm. In this scenario, PI-LSTM delivers more accurate predictions, and the rotor speed curve predicted by PI-LSTM closely follows the real curve without steady error, demonstrating its superior ability to handle such transients. In contrast, the LSTM model shows notable deviations, particularly in the early stages of load reduction, where the rotor speed experiences significant drift, and the prediction error is noticeably higher.

Figure 8 shows the response performance of the system under an 80%-60% load decrease. It can be seen that under the effect of power distribution, the SOFC power remains basically unchanged after an instantaneous change, and the gas turbine quickly reduces its load to 10MW to maintain stable. The maximum overshoot is 70rpm. However, from the prediction performance, although the LSTM has a relatively good fitting accuracy in the above-mentioned gas turbine power, SOFC power, and efficiency, there is a prediction error of a large instantaneous overshoot in speed prediction, reaching 20rpm, and also there is a steady-state prediction error lasting up to 100s.

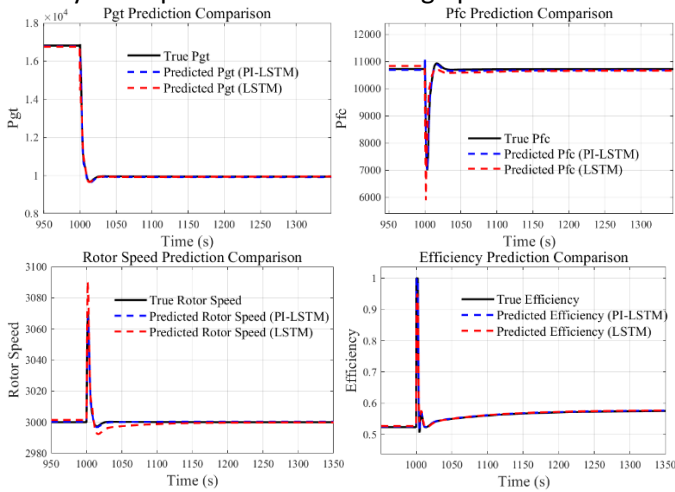


Fig. 8 Prediction Characteristics of SOFC, GT Power, Generation rotor speed, and efficiency based on PI-LSTM and LSTM under 80%-60% load variation

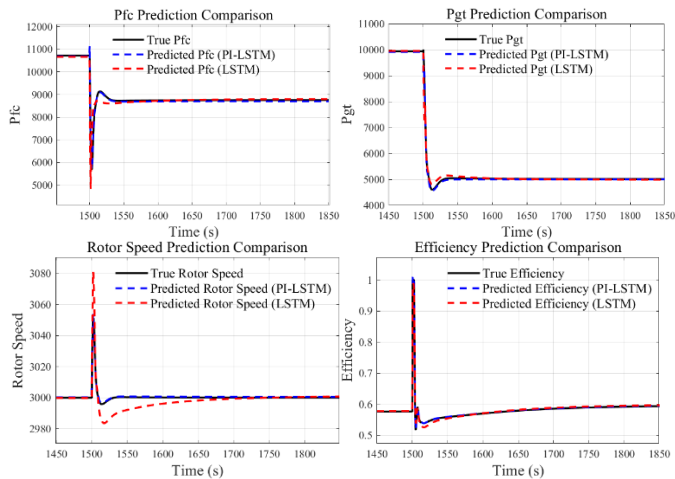


Fig. 9 Prediction Characteristics of SOFC, GT Power, Generation rotor speed, and efficiency based on PI-LSTM and LSTM under 60%-40% load variation

It can be seen from Figure 9 that when the load decrease to 40%, the rotor speed error under the LSTM prediction further increases, with an overshoot prediction error of ± 30 rpm, and the settling time error is as long as 150 seconds. Figure 10 presents the dynamic error curves and R^2 values for both models under

continuously load decreasing, providing insight into their performance over the entire simulation period. The dynamic error curve reveals that PI-LSTM maintains a small and steady error within 5 rpm, while LSTM experiences considerable fluctuation, especially during load changes. The maximum error for LSTM exceeds 30 rpm (1%), which is significantly higher than that of PI-LSTM.

The dynamic R^2 curve further highlights the robustness of PI-LSTM, with its R^2 consistently above 97.5%, indicating strong model fit and stability. In contrast, LSTM's R^2 drops dramatically during load transients, with the minimum value reaching as low as 40%, reflecting a significant loss in prediction accuracy and generalization capability. In summary, it can be seen that the PI-LSTM proposed in this paper not only maintains high accuracy during training, but also maintains strong stability and robustness during actual large load mutation processes due to the physical constraint equations, achieving high-precision prediction of transient system performance.

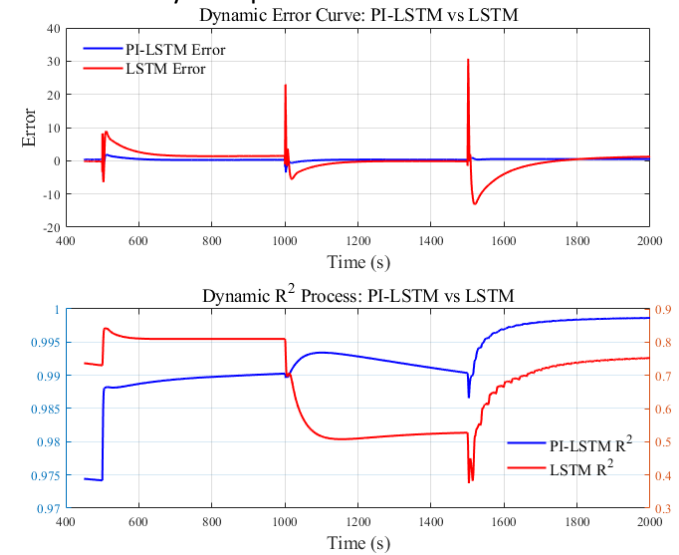


Fig. 10 Comparison between Dynamic Error and R^2

5. CONCLUSION This study introduces a novel Physics-Informed Long Short-Term Memory (PI-LSTM) approach for predicting the dynamic behavior of marine IRGT/SOFC hybrid systems in all-electric propulsion. By incorporating physical constraints, such as rotor speed dynamics, into the LSTM model, we significantly improve the accuracy and robustness of transient predictions. The PI-LSTM model outperforms conventional LSTM and BP models, reducing errors in key system parameters like output power, rotor speed, and efficiency.

Key contributions include:

The PI-LSTM model has significantly improved the prediction accuracy of key system parameters. The RMSE

of the system output power has decreased from 107 to 52, the RMSE of the gas turbine power has dropped from 183 to 83, the RMSE of the rotor speed has reduced from 2.08 to 1.05, and the R^2 value has increased from 0.926 to 0.998, which proves the effectiveness of physical constraints.

Under continuously sudden load decrease, PI-LSTM can control the error of rotor speed within a maximum of 5 revolutions per minute, while the error of the traditional LSTM model is as high as 30 revolutions per minute, demonstrating the superiority of PI-LSTM in handling sudden load changes.

PI-LSTM not only achieves excellent performance in the system of this study, but also has strong adaptability. It can be widely applied to other marine hybrid power systems and has good scalability.

In conclusion, the PI-LSTM framework provides a promising pathway for enhancing the predictive capabilities of marine hybrid propulsion systems, ensuring more accurate and reliable operation under diverse operational conditions. Given its adaptability and robustness, this method can be extended to other energy systems and can play a crucial role in the future of maritime electrification, facilitating the transition toward more sustainable and efficient marine transportation.

ACKNOWLEDGEMENT

The research is supported by National Natural Science Foundation of China under Grant No. (52176013), Shanghai Inter-governmental International Cooperation Project No. (23160710200), National Science and Technology Major Project (J2019-I-0012-0012). And by the UK Royal Society under Grant IES\R3\213195.

REFERENCE

[1] IMO. "Revised GHG Strategy for Global Shipping." <https://www.imo.org/en/OurWork/Environment/Pages/2023-IMO-Strategy-on-Reduction-of-GHG-Emissions-from-Ships.aspx> (accessed).

[2] Z. Wang, P. Liao, F. Long, Z. Wang, Y. Ji, and F. Han, "Maritime electrification pathways for sustainable shipping: Technological advances, environmental drivers, challenges, and prospects," *eTransportation*, vol. 26, p. 100462, 2025/12/01/ 2025, doi: <https://doi.org/10.1016/j.etrans.2025.100462>.

[3] H. Daniel, J. P. F. Trovão, and D. Williams, "Shore power as a first step toward shipping decarbonization and related policy impact on a dry bulk cargo carrier," *eTransportation*, vol. 11, p. 100150, 2022, doi: 10.1016/j.etrans.2021.100150.

[4] S. Guo, Y. Wang, L. Dai, and H. Hu, "All-electric ship operations and management: Overview and future research directions," *eTransportation*, vol. 17, p. 100251, 2023/07/01/ 2023, doi: <https://doi.org/10.1016/j.etrans.2023.100251>.

[5] R. Zamotorin, R. Kurz, Z. Donghui, M. Lubomirsky, and K. Brun, "Control Optimization for Multiple Gas Turbine Driven Compressors," *Volume 9: Oil and Gas Applications; Supercritical CO₂ Power Cycles; Wind Energy*, 2018.

[6] O. B. Ogar, S. Nitonye, and I. John-Hope, "Design Analysis and Optimal Matching of a Controllable Pitch Propeller to the Hull and Diesel Engine of a CODOG System," *Journal of power and energy engineering*, vol. 6, no. 3, pp. 53-74, 2018, doi: 10.4236/jpee.2018.63005.

[7] J. Li and M. Deng, "Energy Optimal Operation Strategy of Ship Power Station with Multi Energy," 2021: IEEE, pp. 1485-1489, doi: 10.1109/EI252483.2021.9713349.

[8] A. Ashar, L. Wehrle, O. Deutschmann, and R. J. Braun, "High performance ammonia-fueled SOFC hybrid system for decarbonizing heavy-duty transportation applications," *Applied Energy*, vol. 390, p. 125788, 2025/07/15/ 2025, doi: <https://doi.org/10.1016/j.apenergy.2025.125788>.

[9] Y. Li, Y. Weng, and S. Weng, "Part-load, startup, and shutdown strategies of a solid oxide fuel cell-gas turbine hybrid system," *Front Energy*, vol. 5, no. 2, pp. 181-194, 2011, doi: 10.1007/s11708-011-0149-7.

[10] M. A. Azizi and J. Brouwer, "Progress in solid oxide fuel cell-gas turbine hybrid power systems: System design and analysis, transient operation, controls and optimization," *Applied Energy*, vol. 215, no. APR.1, pp. 237-289, 2018.

[11] P. Kumar and O. Singh, "A review of solid oxide fuel cell based hybrid cycles," *International journal of energy research*, no. 7, p. 46, 2022.

[12] A. L. Dicks and D. A. J. Rand, *Fuel Cell Systems Explained (3rd Edition)*, Third edition ed. Newark: Newark: John Wiley & Sons, 2018.

[13] M. Minutillo, A. Perna, and E. Jannelli, "SOFC and MCFC system level modeling for hybrid plants performance prediction," *International journal of hydrogen energy*, vol. 39, no. 36, pp. 21688-21699, 2014, doi: 10.1016/j.ijhydene.2014.09.082.

[14] X. Mi *et al.*, "Quick-safe intelligent control strategy for SOFC/GT all-electric ship propulsion system under pulsed load using EO-NN approach," *Energy*, vol. 333, p. 137490, 2025/10/01/ 2025, doi: <https://doi.org/10.1016/j.energy.2025.137490>.

[15] X.-l. Wu *et al.*, "Performance prediction of gasification-integrated solid oxide fuel cell and gas turbine cogeneration system based on PSO-BP neural

network," *Renewable Energy*, vol. 237, p. 121711, 2024/12/01/ 2024, doi: <https://doi.org/10.1016/j.renene.2024.121711>.

[16]C. Jinwei, H. Zhenchao, and H. Zhang, "Study on an adaptive multi-model predictive controller for the thermal management of a SOFC-GT hybrid system," *E3S Web of Conferences*, vol. 414, p. 02013, 08/25 2023, doi: 10.1051/e3sconf/202341402013.

[17]B. J. Spivey and T. F. Edgar, "Dynamic modeling, simulation, and MIMO predictive control of a tubular solid oxide fuel cell," *Journal of Process Control*, vol. 22, no. 8, pp. 1502-1520, 2012/09/01/ 2012, doi: <https://doi.org/10.1016/j.procont.2012.01.015>.

[18]R. Panday, N. F. Harun, B. Zhang, D. Maloney, D. Tucker, and S. Bayham, "Analyzing Gas Turbine-Generator Performance of the Hybrid Power System," *IEEE Transactions on Power Systems*, vol. 37, no. 1, pp. 543-550, 2022, doi: 10.1109/TPWRS.2021.3091964.

[19]V. Haji Haji, A. Fekih, C. A. Monje, and R. Fakhri Asfestani, "Adaptive model predictive control design for the speed and temperature control of a V94.2 gas turbine unit in a combined cycle power plant," *Energy*, vol. 207, p. 118259, 2020/09/15/ 2020, doi: <https://doi.org/10.1016/j.energy.2020.118259>.

[20]A. Nguembang Fadja *et al.*, "Machine Learning Approaches for the Prediction of Gas Turbine Transients," *Journal of Computer Science*, vol. 20, pp. 495-510, 05/01 2024, doi: 10.3844/jcssp.2024.495.510.

[21]https://military-history.fandom.com/wiki/Type_052D_destroyer. "Type 052D destroyer." https://military-history.fandom.com/wiki/Type_052D_destroyer (accessed).

[22]J. Wen *et al.*, "Optimal power allocation strategy and characteristic analyze of parallel IRGT/SOFC system for large ocean-going vessel under multi-scenario operation," *Applied Energy*, vol. 401, p. 126676, 2025/12/15/ 2025, doi: <https://doi.org/10.1016/j.apenergy.2025.126676>.

[23]J. Wen, S. Zhang, J. Lu, C. Spataru, Y. Weng, and X. Lv, "Coordinated intelligent control strategy and power management for marine gas turbine under pulsed load using optimized neural network," *Energy*, p. 133719, 2024/11/08/ 2024, doi: <https://doi.org/10.1016/j.energy.2024.133719>.

[24]B. energy. "Load Following Solid Oxide Fuel Cell " <https://www.bloomenergy.com/wp-content/uploads/load-following-solid-oxide-fuel-cell.pdf> (accessed).

[25]X. Mi, J. Wen, J. Yang, C. Spataru, Y. Weng, and X. Lv, "Safety and fast-tracking assessment of an innovative SOFC/GT all-electric ship propulsion system under pulsed

load," *Applied Thermal Engineering*, vol. 270, p. 126246, 2025/07/01/ 2025, doi: <https://doi.org/10.1016/j.applthermaleng.2025.126246>.

[26]P. Aguiar, C. S. Adjiman, and N. P. Brandon, "Anode-supported intermediate-temperature direct internal reforming solid oxide fuel cell - II. Model-based dynamic performance and control," *J POWER SOURCES*, vol. 147, no. 1-2, pp. 136-147, 2005, doi: 10.1016/j.jpowsour.2005.01.017.